DISCLAIMER

This report was prepared as an account of work sponsored by an agency of the United States Government. Neither the United States Government nor any agency thereof, nor any of their employees, makes any warranty, express or implied, or assumes any legal liability or responsibility for the accuracy, completeness, or usefulness of any information, apparatus, product, or process disclosed, or represents that its use would not infringe privately owned rights. Reference herein to any specific commercial product, process, or service by trade name, trademark, manufacturer, or otherwise does not necessarily constitute or imply its endorsement, recommendation, or favoring by the United States Government or any agency thereof. The views and opinions of authors expressed herein do not necessarily state or reflect those of the United States Government or any agency thereof. Reference herein to any social initiative (including but not limited to Diversity, Equity, and Inclusion (DEI); Community Benefits Plans (CBP); Justice 40; etc.) is made by the Author independent of any current requirement by the United States Government and does not constitute or imply endorsement, recommendation, or support by the United States Government or any agency thereof.

LA-UR-25-30563

Approved for public release; distribution is unlimited.

Title:	Ion irradiation testing of 14YWT ODS and HT-9
Author(s):	Kim, Hyosim Schneider, Matthew M. Gordon, Emma Ansley Massey, Caleb Eftink, Benjamin P.
Intended for:	Report
Issued:	2025-10-23

Ion irradiation testing of 14YWT ODS and HT-9

Fuel Cycle Research & Development

Prepared for
U.S. Department of Energy
Advanced Fuels Campaign

Hyosim Kim, Matt Schneider,
Emma Gordon, Caleb Massey,
Benjamin Eftink

09/30/2025

SUMMARY

Ion irradiations were performed to compare a new generation of 14YWT, NFA-2, to the prior generation NFA-1. Irradiations were performed at 450 °C and to a peak dose of 500 dpa. The irradiation condition was chosen as a relevant temperature for scoping for an upcoming JOYO neutron irradiation, and the high dose was chosen to evaluate the exceptional microstructural stability to irradiation induced changes of 14YWT. For comparison, HT-9 was irradiated as the benchmark. Irradiation induced changes to the microstructures were limited for the 14YWT samples and extensive for the HT-9 benchmark.

TABLE OF CONTENTS

Intentionally Blank

1. Introduction

Cladding materials for fast neutron spectrum reactors are subjected to irradiation, elevated temperatures and corrosive environments. The current benchmark cladding material is HT-9 ferritic/martensitic steel for its lower irradiation swelling response and higher thermal conductivity than austenitic stainless steels. Both austenitic and ferritic/martensitic steels have been demonstrated as metallic fuel cladding in the EBR-II sodium cooled fast reactor. Cladding performance could be improved further for better reactor economics, for example, by increasing irradiation creep strength and decreasing swelling compared to HT-9. Nano-ferritic alloys (NFAs) are being developed specifically for high temperature irradiation environments as an improvement to HT-9. These NFAs utilize a uniform distribution of nano-scale oxide particles both strength and increasing irradiation defect recombination sites.

Ion irradiation using accelerated particles is a lower cost alternative to neutron irradiations when studying radiation-induced damage in structural materials due to its ability to produce high displacement damage and defect structures in accelerated time scales. Such experiments allow systematic variation of temperature, dose rate, and ion species under well controlled laboratory conditions, while avoiding issues of activation, high costs, and limited availability associated with reactor neutron sources. For example, intermediate energy proton or heavy ion beams have been used to closely reproduce some microstructural features observed in neutron irradiated materials [2-4, Zhu 2024]. However, there are limitations. Ion irradiation produces damage profiles that are often confined to near surface layers, lacks the full spectrum of transmutation reactions found under neutron irradiation, and typically involves much higher damage rates, potentially leading to dose rate effects that do not scale directly with reactor conditions [2]. The limited irradiated volume requires careful sample preparation and analysis and potential contamination during irradiation can also distort observed property changes [5-8]. A multi-institutional active effort to demonstrate the potential of ion irradiations for material qualification is the DOE funded Grand Challenge IRP Simulating Neutrons with Accelerated Particles (SNAP).

In this study, high dose irradiations were performed on a prior and new generation of 14YWT, and compared to HT-9. Best practices were implemented using a W and Ag coating method to minimize carbon contamination, drawing on lessons learned from previous studies [9-11]. The thin coating layers on the sample surface effectively can block the carbon especially during extended period of ion irradiation and prevent potential carbide formation within the irradiated region. Carbon atoms injected during irradiation also hinder void formation and impede accurate measurement [9]. By coating Ag on the specimen surface, carbon atoms can be blocked due to extremely low carbon mobility in Ag and the W layer is coated on top of Ag to prevent sputtering during long ion irradiation. These layers (~200 nm) will slightly reduce the irradiated volume within the sample, but no intermetallic formation or chemical interaction was observed between the coating layers and the specimen. As safe analysis depth is located at deeper region to avoid surface effect [12], the interface between the coating and the specimen also typically does not affect measurements.

2. Materials and Methods

2.1. Sample Preparation

Two different variants of 14YWT (NFA-1 and NFA-2) and one HT-9 sample were prepared for high dose ion irradiation, their compositions are summarized in Table 1. 14YWT NFA-2 was developed by ORNL and the manufacturing details can be found in [1], two samples of this variant were irradiated, 2-1 and 2-2, which are effectively the same. The other 14YWT sample is NFA-1 that was developed as part of the DOE Fuel Cycle Research and Development Program through a collaboration between LANL, ORNL and University of California, Santa Barbara. Precursor powder for NFA-1 was produced via gas atomization by ATI Powder Metals Laboratory and mechanically alloyed and consolidated at ORNL. The NFA-1 sample was from pilger processed tubing with intermediate annealing at 1200 ℃. Further manufacturing and processing details for NFA-1 can be found in [13].

Specimens were mounted in the epoxy and polished using SiC grit paper up to P-4000, and then with 3 and 1 μm diamond solutions on a polishing cloth to remove cold-worked surface material from machining. For the final polishing step, the specimens except the CEA pilgered NFA-1 were polished using a Vibromet over 24 hours in a 0.05 μm colloidal alumina or silica suspension. After polishing, specimens were soaked in acetone to remove the epoxy, and sonicated in acetone for 10 minutes to remove any residue from the polishing process. The CEA pilgered NFA1 sample was electropolished using a twin jet electropolisher with 5 % perchloric acid and 95 % methanol solution at around -30 ℃ to remove any cold-worked layer caused by previous polishing steps.

Table 1 Compositions of materials in wt%.

Elements	Fe	Cr	W	Ti	Y	Y_2O_3	Mo	Al	Ni	Mn	V	Si	C	P	O	N	S
NFA 2-1 and 2-2	Bal.	13.89	2.97	.3	-	.3	-	.024	.015	.074	-	.021	.0063	.008	.0079	.0111	.004
Pilgered NFA-1	Bal.	14	3	.4	.21		-	-	-	-	-	-	-	-	-	-	-
HT-9	Bal.	11.42	.48	-	-		1.00	-	.52	.56	.30	.26	.20	<.01	.007	.044	.001

All specimens were coated with 60 nm of Ag and 140 nm of W using a magnetron sputtering coating system at LANL (MPA-CINT) after polishing and prior to irradiation to prevent carbon inflow during ion irradiation. This method was demonstrated by other studies [9-11] and effectively blocked carbon to achieve more accurate irradiation results. Carbon atoms have extremely low mobility in Ag and the outer W layer protects the Ag layer from sputtering during ion irradiation.

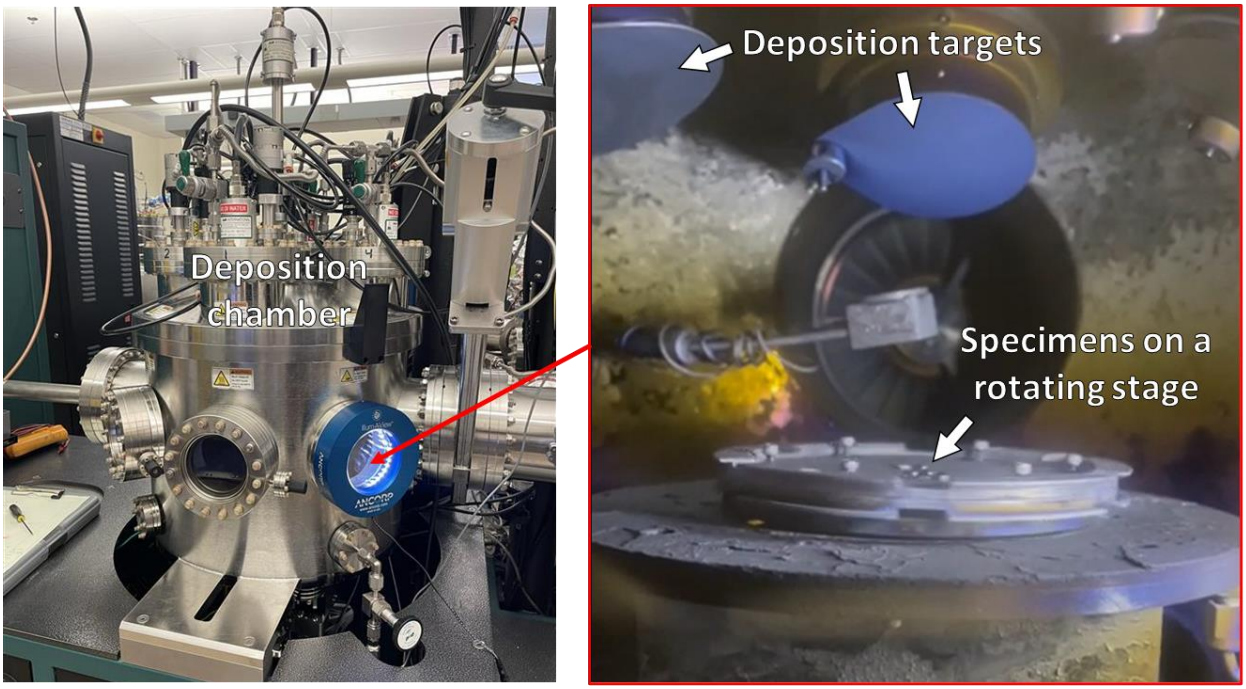

Figure 1 CINT magnetron sputtering coating chamber and the samples on the rotating stage located inside the chamber.

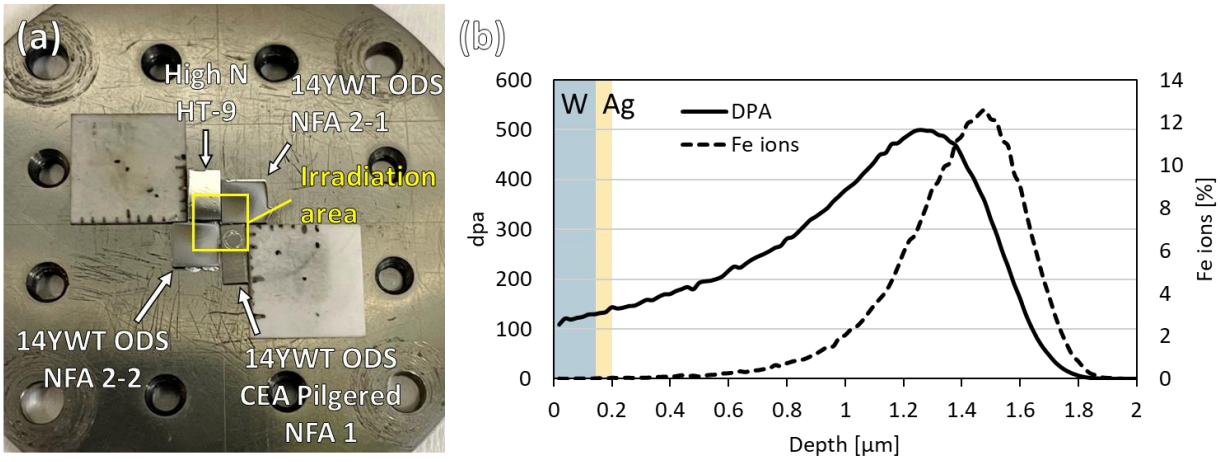

Figure 2 (a) Specimens mounted on the stage for ion irradiation using a silver paste and (b) profiles of 5 MeV Fe dpa and Fe ions in 14YWT calculated using SRIM-2013. W and Ag layers are superimposed on the SRIM figure.

The ion irradiation was conducted at the Ion Beam Materials Laboratory (IBML) at LANL using a NEC 3 MV tandem accelerator. Four specimens were irradiated using a 5 MeV Fe^{2+} defocused beam to 500 peak displacement-per-atom (dpa) at 450 °C to emulate reactor environment. Higher ion beam energy is preferrable to increase penetration depth and to minimize surface effect and injected interstitial effect, but the 5 MeV was the highest energy achievable at the moment due to unstable accelerator terminal voltage. The 500 peak dpa is equivalent to 5.03×10^{17} ions/cm^2 and the dose rate was kept in the 10^{-3} dpa/s level. Figure 1a shows the sample layout on the stage, and the irradiation area is marked with the yellow square. Fluence and dpa were calculated using Stopping and Range of Ion in Matter (SRIM) 2013 with the Kinchin-Pease option and the results are shown in figure 1b. Displacement energies used are 40 eV for Fe and Cr, 90 eV for W, 36 eV for Y, and 30 eV for Ti [14]. 5 MeV Fe beam penetrates about 1.9 μm as shown in the figure 1b.

Post-irradiation characterization was conducted using a Thermo Fisher Spectra Ultra transmission electron microscope (TEM) at electron microscopy laboratory (EML) in LANL. TEM foils were prepared using a focused ion beam (FIB) lift-out technique. During the FIB process, a Pt or W layer was deposited on the specimen surface to protect the irradiated surface and the 30 kV Ga beam was used to etch and polish the foil. Final clean-up polishing was conducted on the foils to remove FIB damage using 8, 5, and 2 kV Ga beams. TEM bright-field (BF), scanning TEM (STEM), high-angle annular dark-field (HAADF), selected area diffraction pattern (SAED), and energy dispersive X-ray spectroscopy (EDS) were used for sample characterization.

3. Results and Discussion

Characterization of the three types of samples will be presented below. Starting with the two NFA-2 14YWT samples, then the NFA-1 14YWT, and lastly the HT-9. Key observations for each will be provided and a comparison between all of the samples will be presented in the conclusions.

3.1 NFA-2 14YWT TEM characterization

Both 2-1 and 2-2 samples showed similar post irradiation features. TEM observation looked for changes in precipitates, elemental distribution, and grains. The results are shown in the micrographs in Figures 3 though 5.

There were two types of precipitates observed, Ti rich precipitates on the order of 50 nm in size and smaller Y and Ti rich oxides ranging from several to around 20 nm in size. For the Ti rich precipitates, for both the 2-1 and 2-2 samples, the irradiations decreased their prevalence. The decreased presence in the irradiated regions suggests they are not stable during the irradiation conditions of this study. Figure 3 shows an EDS map showing the difference in the larger Ti rich precipitates between the irradiated and non-irradiated regions. Small size, less than 20 nm, and higher number density Y-Ti-O particles were observed at grain boundaries, Figure 4. The EDS maps do not show the oxides around 1.9 nm that were reported for the starting material since the TEM foil was too thick. These precipitates are likely the cause of the grain stability at these irradiation conditions.

Compositional changes were observed at the grain boundaries in the irradiated regions. Both Cr and W had higher concentrations at the grain boundaries than the matrix grains. While Fe was depleted at the grain boundaries. Compositional segregation is common for ion irradiated steels at elevated temperatures.

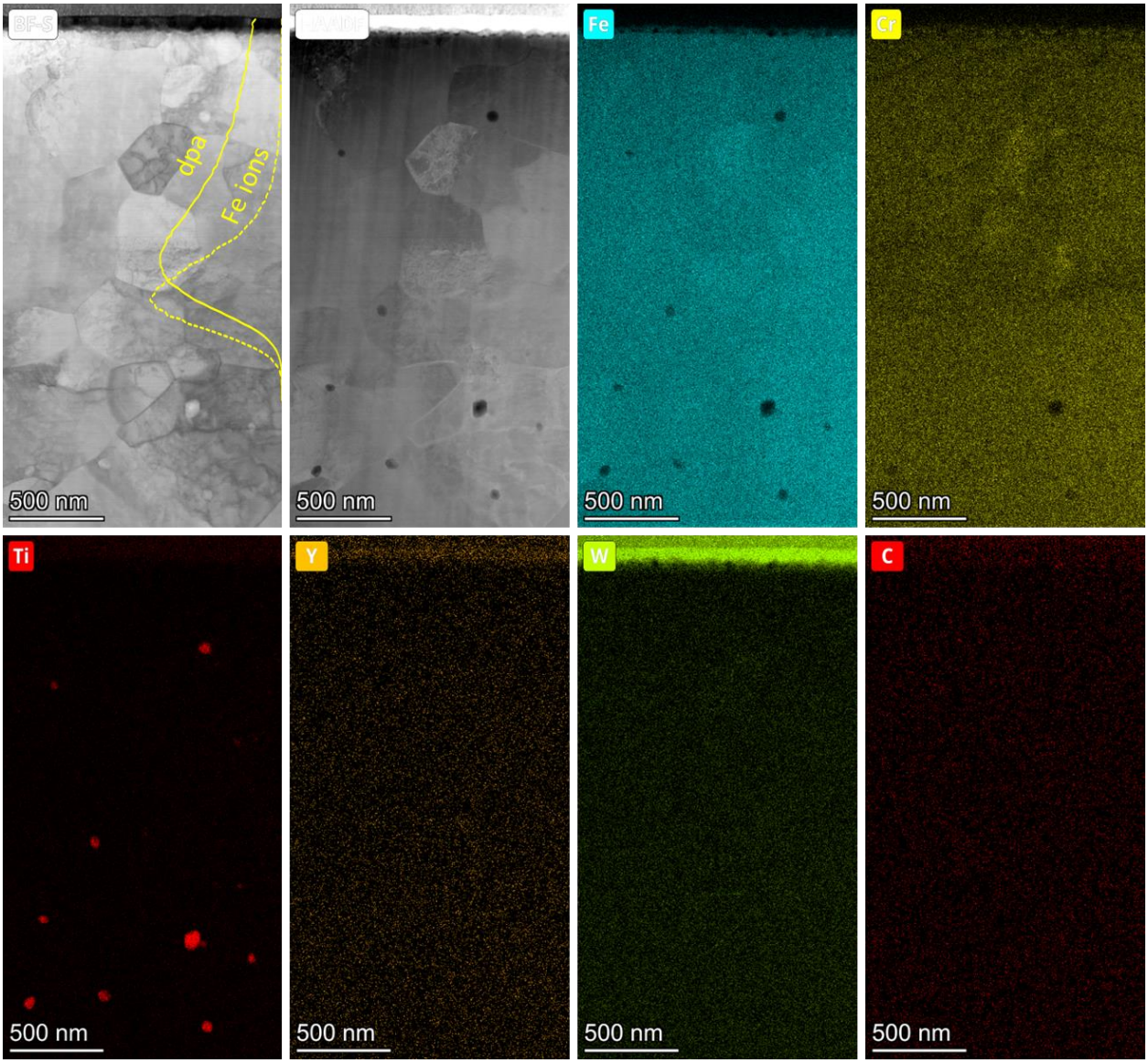

Figure 3 TEM bright field, STEM HAADF images, and EDS elemental maps of irradiated 14YWT NFA2-2 specimen. SRIM profiles are superimposed on the BF image. Large Ti-rich precipitates were found in both irradiated and unirradiated regions, but with a lower density in the irradiated region. Slight Cr depletion was observed at grain boundaries within the irradiated region.

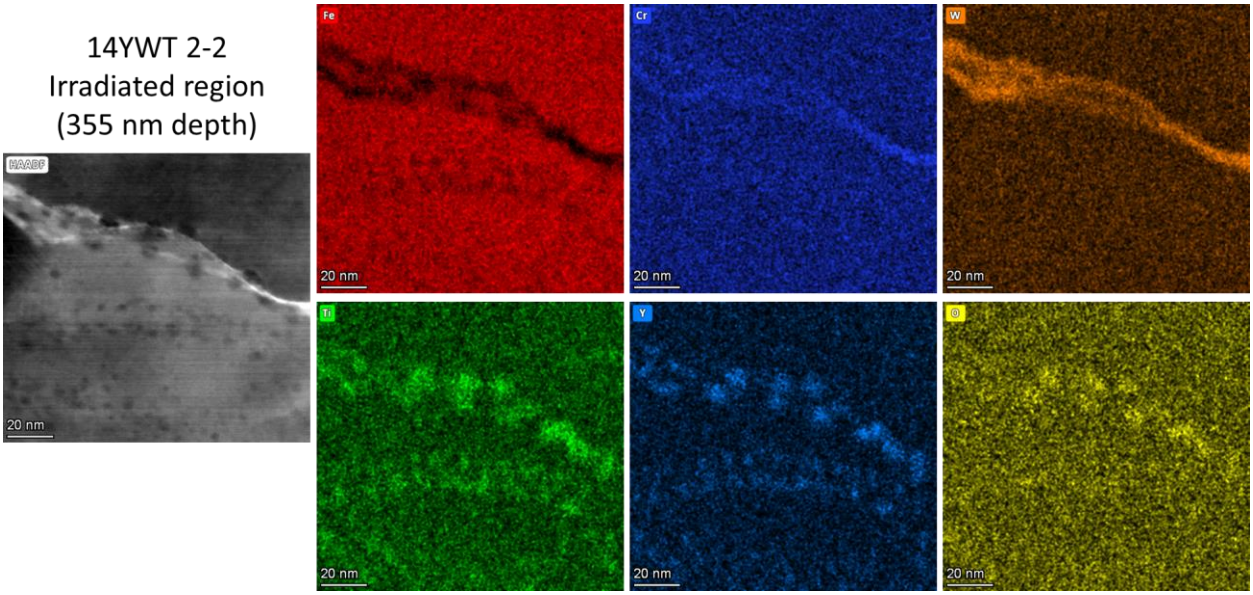

Figure 4 STEM HAADF image and EDS elemental maps of irradiated 14YWT NFA2-2 specimen obtained from 355 nm depth from the surface (within the irradiated region). Cr and W segregation was observed at the grain boundary and small size Y-Ti-O particles were observed at the grain boundary.

3.2 NFA-1 14YWT TEM characterization

The NFA-1 material showed similar behavior to the NFA-2 in terms of precipitates, grain stability and elemental segregation at the grain boundaries. Figure 5 shows STEM HAADF in addition to EDS elemental maps for NFA-1 14YWT. In this sample, however, the larger Ti precipitates were not prevalent enough to determine if they are unstable during irradiation. When observing the Y in Figure 5, precipitates were observed in both the irradiated and non-irradiated regions with sizes from several nanometers to the largest around 100 nm. The Y rich precipitates appear to be relatively unchanged by the irradiation, but would require atomic resolution TEM to confirm. Additionally, the grains do not appear to have qualitatively grown.

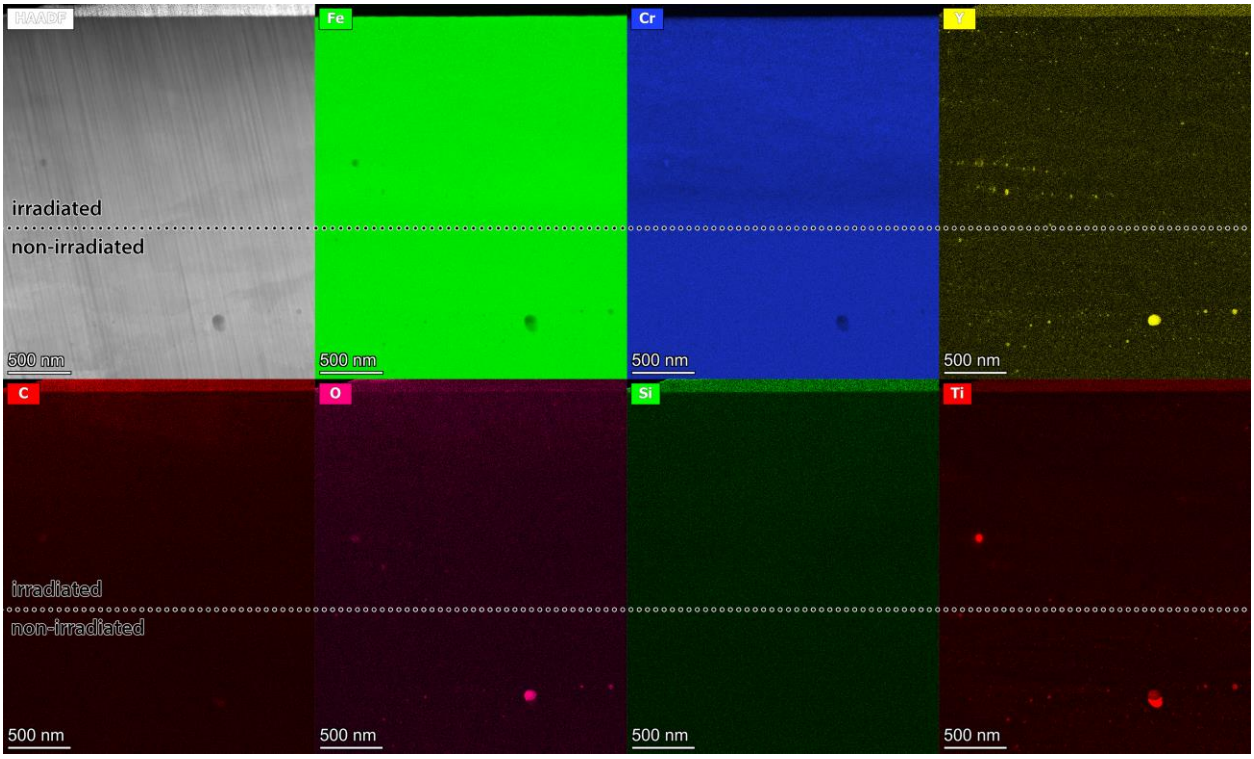

Figure 5 TEM BF, STEM HAADF image and EDS elemental maps of irradiated 14YWT NFA1 CEA pilgered specimen.

3.3 HT-9 TEM characterization

The irradiated HT-9 ferritic/martensitic steel showed compositional segregation and larger than expected grain structure. In this material a lath structure organized into packets and prior austenite grains is expected, however, was not observed. There are a few possible explanations for this unexpected result: 1) the TEM sample was taken from a region of delta ferrite or 2) the irradiation dose and temperature combination resulted in substantial grain growth. From Figure 7 there is evident precipitation of Ni and Cr precipitates. Ni rich precipitation are also Si rich indicating G-phase. The Cr precipitates have increased C indicating carbides. The non-irradiated region has a relatively uniform elemental distribution.

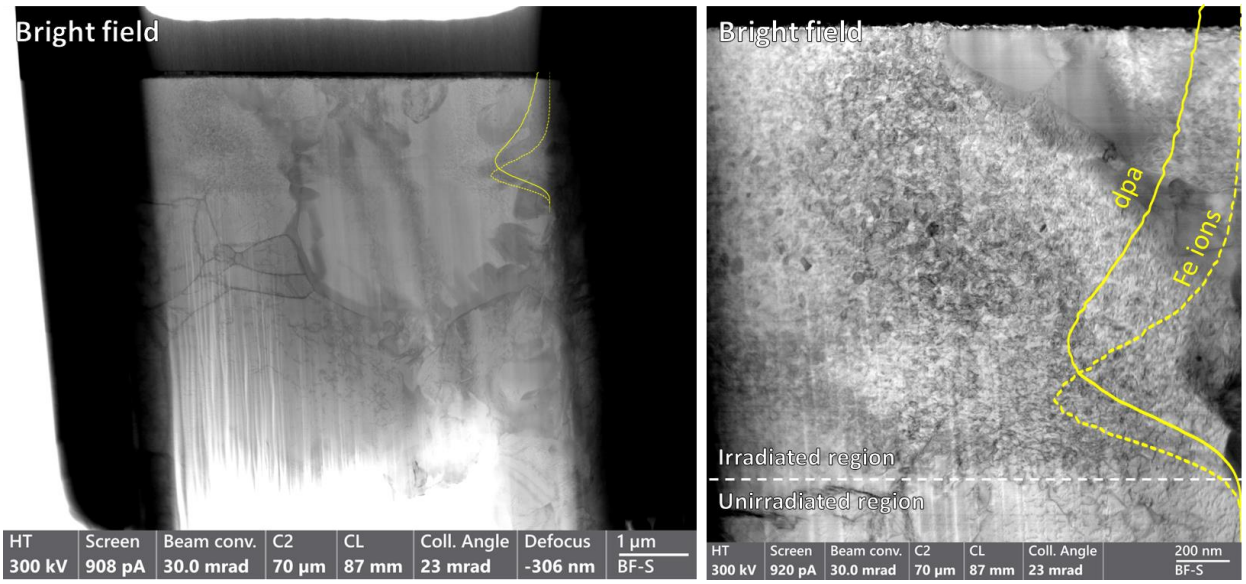

Figure 6 TEM BF images of irradiated high N HT9 specimen. SRIM profiles are superimposed on both BF images to show irradiated regions.

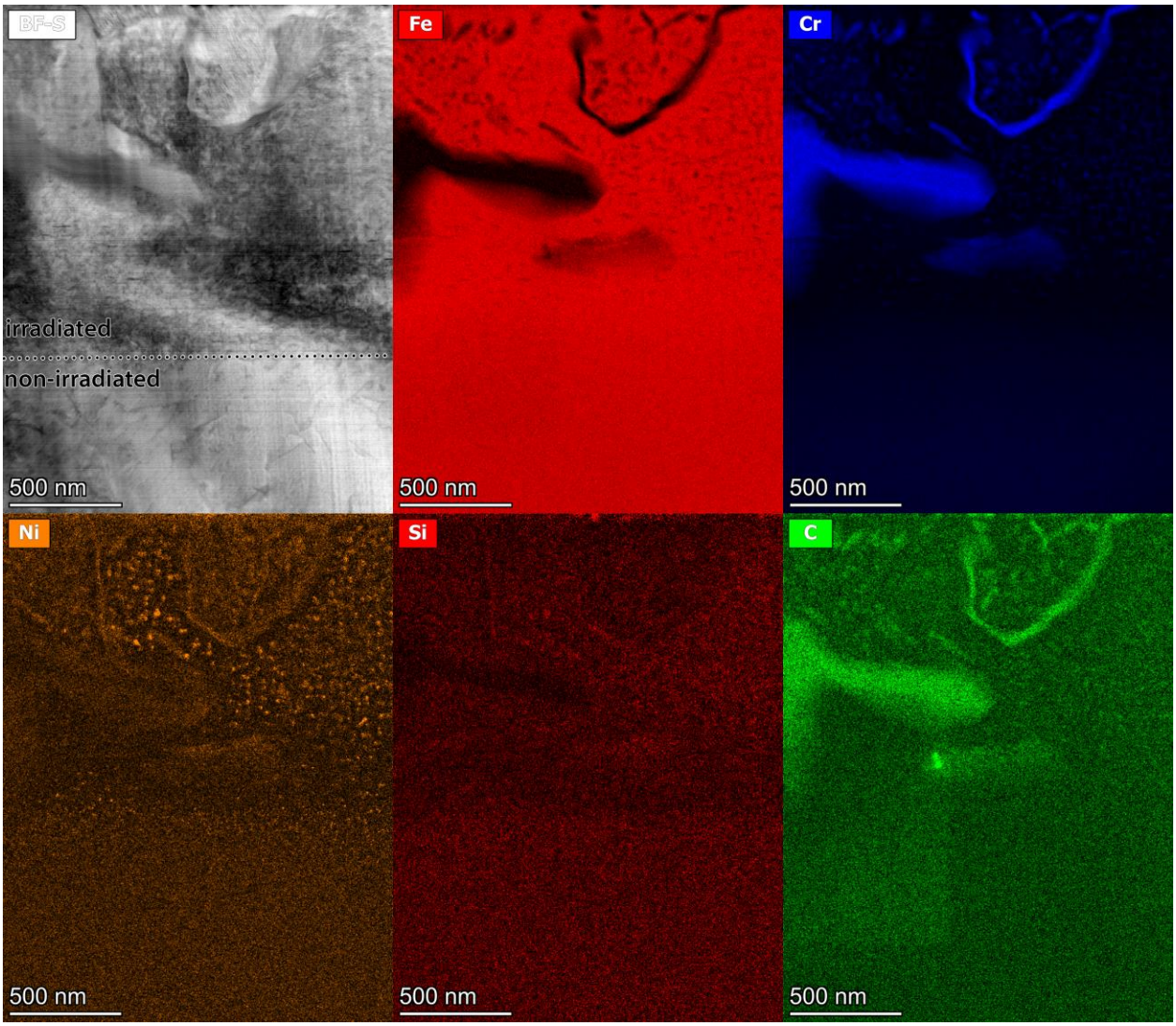

Figure 7 TEM BF and EDS elemental maps of irradiated high N HT9 specimen.

4. Conclusions

Both 14YWT variants, NFA-1 and NFA-2, had similar microstructural changes from self-ion irradiation at 450 °C to a peak of 500 dpa. Minor elemental segregation was observed at the grain boundaries and both exhibited relatively unchanged grain size. Larger Ti rich precipitates in NFA-2 were observed to not be stable under these irradiation conditions. The HT-9 sample showed significantly more compositional segregation and additional precipitates, G-phase and Cr carbides, compared to the 14YWT samples. The HT-9 sample also had larger than expected grains, which is unclear whether this was due to the sample being from a region of delta ferrite or the high dose and temperature.

5. References

1. Massey, Hoelzer, ORNL report.
2. G.S. Was, Challenges to the use of ion irradiation for emulating reactor irradiation, J. Mater. Res. 30 (2015) 1158–1182.
3. S. Jepeal, L. Snead, Z. Hartwig, Intermediate energy proton irradiation: rapid, high-fidelity materials testing for fusion and fission energy systems, arXiv:2009.00048 (2020).
4. K.C. Polavaram, S.K. Evani, S.M. Drewry, et al., Silicon ion radiation as a viable surrogate for emulating neutron radiation damage in silicates, npj Mater. Degrad. 8 (2024) 89.
5. G.S. Was, S. Taller, Z. Jiao, A.M. Monterrosa, D. Woodley, D. Jennings, T. Kubley, F. Naab, O. Toader, E. Uberseder, Resolution of the carbon contamination problem in ion irradiation experiments, Nucl. Instrum. Methods Phys. Res. B 412 (2017) 58–65.
6. J. Wang, M.B. Toloczko, K. Kruska, D.K. Schreiber, D.J. Edwards, Z. Zhu, J. Zhang, Carbon contamination during ion irradiation—accurate detection and characterization of its effect on microstructure of ferritic/martensitic steels, Sci. Rep. 7 (2017) 15813.
7. J.G. Gigax, H. Kim, E. Aydogan, F.A. Garner, S. Maloy, L. Shao, Beam-contamination-induced compositional alteration and its neutron-atypical consequences in ion simulation of neutron-induced void swelling, Mater. Res. Lett. 5 (2017) 478–485.
8. L. Shao, J. Gigax, D. Chen, H. Kim, F.A. Garner, J. Wang, M.B. Toloczko, Carbon contamination, its consequences and its mitigation in ion-simulation of neutron-induced swelling of structural metals (conference/chapter), in: Proc. 18th Int. Conf. Environmental Degradation of Materials in Nuclear Power Systems — Water Reactors (2017).
9. H. Kim, J.G. Gigax, O. El-Atwani, M.R. Chancey, J.K. Baldwin, Y. Wang, S.A. Maloy, Comparison of void swelling of ferritic-martensitic and ferritic HT9 alloys after high-dose self-ion irradiation, Mater. Charac. 173 (2021) 110908.
10. H. Kim, J.G. Gigax, C.J. Rietema, O. El Atwani, M.R. Chancey, J.K. Baldwin, Y. Wang, S.A. Maloy, Void swelling of conventional and composition engineered HT9 alloys after high-dose self-ion irradiation, J. Nucl. Mater. 560 (2022) 153492.
11. M.B. Toloczko, J. Wang, Report on 20-70 dpa(n) preconditioned materials irradiated to 350-500 dpa total dose by ions, June 2019 PNNL-28808.
12. Y. Li, A. French, Z. Hu, A. Gabriel, L.R. Hawkins, F.A. Garner, L. Shao, A quantitative method to determine the region not influenced by injected interstitial and surface effects during void swelling in ion-irradiated metals, J. Nucl. Mater. 573 (2022) 154140.
13. C. Harvey, O. El Atwani, H. Kim, C. Lavender, M. McCoy, D. Sornin, J. Lewandowski, S.A. Maloy, S. Pathak, Microstructure and micro-mechanical analysis of 14YWT nanostructured ferritic alloy after varying thermo-mechanical processing paths into tubing, Mater. Charac. 171 (2021) 110744.
14. A.Yu. Konobeyev, U. Fischer, Yu.A. Korovin, S.P. Simakov, Evaluation of effective threshold displacement energies and other data required for the calculation of advanced atomic displacement cross-sections, Nucl. Eng. Technol. 3 (2017) 169–175.